Single-Molecule Enzymatic Dynamics

H. Peter Lu *et al.*

Science **282**, 1877 (1998);
DOI: 10.1126/science.282.5395.1877

Science (print ISSN 0036-8075; online ISSN 1095-9203) is published weekly, except the last week in December, by the American Association for the Advancement of Science, 1200 New York Avenue NW, Washington, DC 20005.

References and Notes

1. W. Boynton, in *Protostars and Planets II*, D. Black and M. Matthews, Eds. (Univ. of Arizona Press, Tucson, 1985), pp. 772–787; A. P. Boss, *Science* **241**, 565 (1988).
2. E. Stolper, *Geochim. Cosmochim. Acta* **46**, 2159 (1982).
3. G. J. MacPherson, D. A. Wark, J. T. Armstrong, in *Meteorites and the Early Solar System*, J. F. Kerridge and M. S. Matthews, Eds. (Univ. of Arizona Press, Tucson, 1988), pp. 746–807.
4. H. Nagasawa *et al.*, *Geochim. Cosmochim. Acta* **41**, 1587 (1977).
5. R. N. Clayton, N. Onuma, L. Grossman, T. K. Mayeda, *Earth Planet. Sci. Lett.* **34**, 209 (1977).
6. R. N. Clayton, *Annu. Rev. Earth Planet. Sci.* **21**, 115 (1993).
7. $\delta^{17 \text{ or } 18}O_{SMOW} = \{[(^{17 \text{ or } 18}O/^{16}O)_{sample}/(^{17 \text{ or } 18}O/^{16}O)_{SMOW}] - 1\} \times 1000$ [per mil], where SMOW indicates the standard mean ocean water.
8. R. N. Clayton and T. K. Mayeda, *Geophys. Res. Lett.* **4**, 295 (1977).
9. H. Yurimoto, M. Morioka, H. Nagasawa, *Geochim. Cosmochim. Acta* **53**, 2387 (1989); H. Yurimoto *et al.*, *Antarct. Meteorites* **XVI**, 60 (1991); F. J. Ryerson and K. D. McKeegan, *Geochim. Cosmochim. Acta* **58**, 3713 (1994).
10. K. D. McKeegan, L. A. Leshin, S. S. Russell, G. J. MacPherson, *Science* **280**, 414 (1998).
11. H. Yurimoto, H. Nagasawa, Y. Mori, O. Matsubaya, *Earth Planet. Sci. Lett.* **128**, 47 (1994).
12. S. B. Simon, A. M. Davis, L. Grossman, *Lunar Planet Sci.* **XXVI**, 1303 (1995).
13. The polished sample was coated with 30 nm of gold film for SIMS analysis to eliminate the electrostatic charge on the sample surface. Oxygen isotope ratios were measured with a modified Cameca ims 1270 SIMS of TiTech with a high mass resolution technique. The primary ion beam was mass filtered positive Cs ions accelerated to 10 keV and the beam spot size was ~3 μm in diameter. The primary current was adjusted for each measurement to obtain the count rate of negative ^{16}O ions of $\sim 4 \times 10^5$ cps. A normal-incident electron gun was utilized for charge compensation of the analysis area. Negative secondary ions from the ^{16}O tail, ^{16}O, ^{17}O, ^{16}OH and ^{18}O were analyzed at a mass resolution power of ~6000, sufficient to completely eliminate hydride interference. Secondary ions were detected by an electron multiplier operated in a pulse counting mode, and analyses were corrected for dead time (21 ns). The matrix effect which may cause inter-mineral systematic errors can be checked by comparing the analytical results for terrestrial analogues. We measured oxygen isotope ratios of terrestrial standards with known oxygen isotopic ratio (*11*), SPU (spinel from Russia), anorthite (Miyake-jima, Japan), augite (Takashima, Japan), synthetic gehlenite and synthetic åkermanite. The reproducibility of $^{17 \text{ or } 18}O/^{16}O$ on different analysis points of the same standard was ~5 per mil (1σ). The matrix effect of O isotopic analysis among these minerals was less than 5 per mil (1σ) under our analytical conditions. Therefore, we used the SPU standard to obtain O isotope ratio of all the CAI minerals. Overall errors in the measurements are estimated to be ~ 5 per mil (1σ) for each analysis. An average isotope ratio of the SPU standard was used to determine $\delta^{17 \text{ or } 18}O_{SMOW}$ values for corresponding unknown samples. The δ^{17} or $^{18}O_{SMOW}$ values were calculated as follows:

$$(\delta^{17 \text{ or } 18}O_{SMOW})_{uk} = (\delta^{17 \text{ or } 18}O_{SMOW})_{st} + (R_{uk}/R_{st} - 1) \times 1000 \text{ [per mil]}$$

where R is the measured isotope ratio of $^{17 \text{ or } 18}O/^{16}O$ and subscripts uk and st correspond to unknown and standard samples, respectively. Further details of the analytical procedure and the results will be given elsewhere (M. Ito *et al.*, in preparation). After SIMS analyses, the purity of analyzing area was evaluated by high magnification scanning electron microscopy and by optical microscopy. No submicron phases (such as submicron spinel grains or alteration products) were observed in the sputtered craters of the Cs^+ primary beam.
14. Oxygen-16–enriched melilite grains that were not in contact with normal melilite grain were observed in a coarse-grained CAI from the Allende carbonaceous chondrite [G. L. Kim, H. Yurimoto, S. Sueno, *Lunar and Planet. Sci.* **XXIX**, abstr. 1344, Lunar and Planetary Institute, Houston, CD-ROM (1998)], in fine-grained CAIs from the Semarkona ordinary chondrite (*10*), from the ALH85085 ungrouped chondrite [M. Kimura, A. ElGoresy, H. Palme, E. Zinner, *Geochim. Cosmochim. Acta* **57**, 2329 (1993)], and in an Antarctic micrometeorite [C. Engrand, K. D. McKeegan, L. A. Leshin, *Meteoritics Planet. Sci.* **32**, A39 (1997)].
15. G. P. Meeker, *Meteoritics* **30**, 71 (1995).
16. J. P. Greenwood and P. C. Hess, in *Chondrules and the Plotoplanetary Disk,* R. H. Hewins, R. H. Jones, E. R. D. Scott, Eds. (Cambridge Univ. Press, Cambridge, UK, 1996), pp. 205–211.
17. F. H. Shu, H. Shang, A. E. Glassgold, T. Lee, *Science* **277**, 1475 (1997).
18. H. Yurimoto, A. Yamashita, N. Nishida, S. Sueno, *Geochem. J.* **23**, 215 (1989).

19. We thank E. King for providing 7R-19-1 CAI. Supported by the Kagaku-Gijutsu-Cho and the Monbu-Sho.

10 August 1998; accepted 29 October 1998

Single-Molecule Enzymatic Dynamics

H. Peter Lu, Luying Xun, X. Sunney Xie*

Enzymatic turnovers of single cholesterol oxidase molecules were observed in real time by monitoring the emission from the enzyme's fluorescent active site, flavin adenine dinucleotide (FAD). Statistical analyses of single-molecule trajectories revealed a significant and slow fluctuation in the rate of cholesterol oxidation by FAD. The static disorder and dynamic disorder of reaction rates, which are essentially indistinguishable in ensemble-averaged experiments, were determined separately by the real-time single-molecule approach. A molecular memory phenomenon, in which an enzymatic turnover was not independent of its previous turnovers because of a slow fluctuation of protein conformation, was evidenced by spontaneous spectral fluctuation of FAD.

Recent advances in fluorescence microscopy have allowed studies of single molecules in an ambient environment (*1*, *2*). Single-molecule measurements can reveal the distribution of molecular properties in inhomogeneous systems (*3*–*10*). The distributions, which can be either static (*3*–*7*) or dynamical (*8*–*10*), cannot usually be determined by ensemble-averaged measurements. Moreover, stochastic trajectories of a single-molecule property can be recorded in real time, containing detailed dynamical information extractable through statistical analyses. Single-molecule trajectories of translational diffusion (*11*–*13*), rotational diffusion (*14*), spectral fluctuation (*15*), conformational motion (*16*), and photochemical changes (*17*, *18*) have been demonstrated. Of particular interest is the real-time observation of chemical reactions of biomolecules. Enzymatic turnovers of a few motor protein systems have been monitored in real time (*19*–*21*). In the study reported here, we examined enzymatic turnovers of single flavoenzyme molecules by monitoring the fluorescence from their active sites. Statistical analyses of chemical dynamics at the single-molecule level revealed insights into enzymatic properties.

Flavoenzymes are ubiquitous and undergo redox reactions in a reversible manner (*22*). Cholesterol oxidase (COx) from *Brevibacterium* sp. is a 53-kD flavoenzyme that catalyzes the oxidation of cholesterol by oxygen (*23*) (Scheme 1). The active site of the enzyme (E) involves a flavin adenine dinucleotide (FAD), which is naturally fluorescent in its oxidized form but not in its reduced form. The FAD is first reduced by a cholesterol molecule to $FADH_2$, and is then oxidized by O_2, yielding H_2O_2. The crystal structure of COx (*23*) shows that the FAD is noncovalently and tightly bound to the center of the protein and is surrounded by a hydrophobic binding pocket for cholesterol, which is otherwise filled with 14 water molecules.

A fluorescence image of single COx molecules in their oxidized form (Fig. 1A) was taken with an inverted fluorescence microscope by raster-scanning the sample with a fixed He-Cd laser (442 nm, LiCONiX) focus

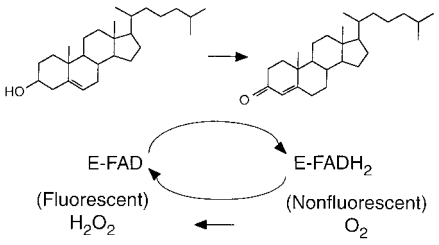

Scheme 1.

H. P. Lu and X. S. Xie, Pacific Northwest National Laboratory, William R. Wiley Environmental Molecular Sciences Laboratory, Richland, WA 99352, USA. L. Xun, Washington State University, Department of Microbiology, Pullman, WA 99164, USA.

*To whom correspondence should be addressed. E-mail: xsxie@pnl.gov

and collecting the FAD emission (peaked at 520 nm) with high efficiency, similar to previous reports (*3, 7, 15*). The single molecules of COx were confined in agarose gel of 99% water (*24*) with no observable translational diffusion. However, the COx molecules were freely rotating within the gel, which was evidenced by a polarization modulation experiment, as previously described (*25*). As the in-plane polarization of the excitation light was modulated between two perpendicular directions at 20 Hz, no emission intensity modulation was seen, indicating that the molecule was freely tumbling at a much faster rate than the modulation frequency. Every COx molecule examined in the gel exhibited the fast rotational diffusion, and thus COx was not bound to the polymer matrix. Ensemble-averaged enzymatic assays for COx (Sigma) in agarose gels yielded turnover rates similar to those in aqueous solutions (*26, 27*). Unlike the enzyme molecules, small substrate molecules (cholesterol and oxygen) undergo essentially free translational diffusion within the gel.

With excess amounts of cholesterol (0.2 mM) and oxygen (saturated solution, 0.25 mM) in the gel, the single FAD emission exhibits on-off behavior (Fig. 1B). We attribute this phenomenon to chemical reactions of the enzyme molecule: Fluorescence turns on and off as the redox state of the flavin toggles between the oxidized (FAD) and reduced ($FADH_2$) states. Each on-off cycle corresponds to an enzymatic turnover. Several control experiments support this conclusion. (i) There is essentially no blinking of emission without cholesterol molecules. Extremely infrequent blinking was seen during long trajectories for only a few, but not all, COx molecules, which we attribute to impurity of substrate molecules or a low-quantum-yield photoinduced process (*1, 4, 17*). (ii) In the presence of cholesterol, the turnover rate is independent of excitation intensity; thus, the blinking is due only to the enzymatic reactions in the ground electronic state rather than photoinduced phenomena. (iii) The averaged turnover rates of the trajectories are the same as the ensemble-averaged turnover rates under similar conditions (*26, 27*).

The length of the trajectories is limited by photobleaching through either photooxidation involving singlet oxygen or excited-state absorption (*1*). We observed a better photostability for the FAD chromophore in protein than for dye molecules, most likely due to the protection by the protein. Trajectories with more than 500 turnovers and 2×10^7 emitted photons (detection efficiency 10%) were recorded; Fig. 1B shows only a portion of a trajectory. During the course of the long trajectories, the average turnover rates (the number of on-off cycles per unit time) did not decrease with time because substrate (cholesterol and oxygen) concentrations were orders of magnitude higher than those of the enzyme. The long trajectories permit detailed statistical analyses.

The most obvious feature of the turnover trajectory in Fig. 1B is its stochastic nature. On a single-molecule basis, the event of a chemical reaction takes place on the subpicosecond time scale and cannot be time resolved here. However, the time needed for diffusion, thermal activation, or both before such an event is usually much longer. The emission on-time and off-time correspond to the "waiting time" for the FAD reduction and oxidation reactions, respectively. The most

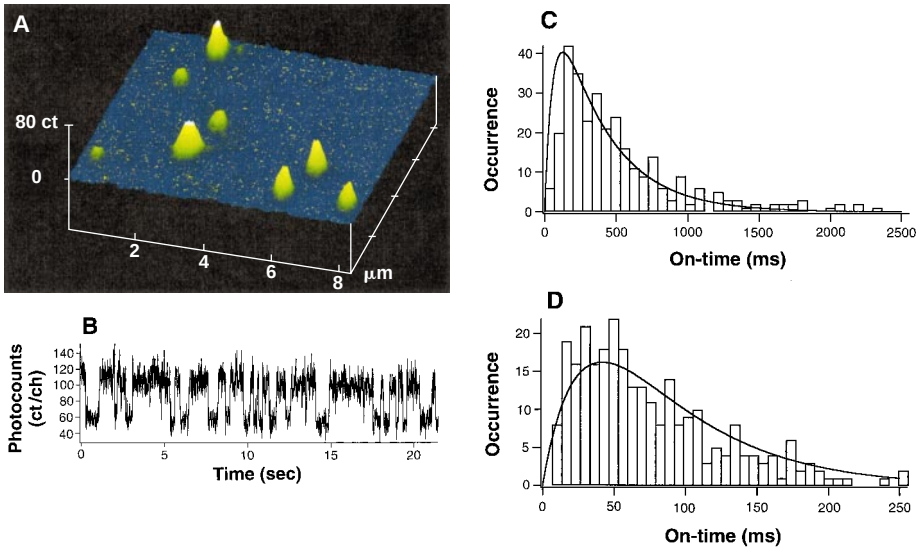

Fig. 1. (**A**) Fluorescence image (8 μm by 8 μm) of single COx molecules immobilized in a 10-μm-thick film of agarose gel of 99% buffer solution (pH 7.4). The emission is from the fluorescent active site, FAD, which is tightly bound to the center of COx. This image was taken in 4 minutes with an inverted fluorescence microscope by raster-scanning the sample with a focused laser beam of 500 nW at 442 nm. Each individual peak is attributed to a single COx molecule. The intensity variation between the molecules is due to different longitudinal positions in the light depths. (**B**) Real-time observation of enzymatic turnovers of a single COx molecule catalyzing oxidation of cholesterol molecules. This panel shows a portion of an emission intensity trajectory recorded in 13.1 ms per channel. Background level is ~50 counts per channel (not subtracted). The trajectory was recorded with a cholesterol concentration of 0.2 mM and saturated oxygen concentration of 0.25 mM. The emission exhibits stochastic blinking behavior as the FAD toggles between oxidized (fluorescent) and reduced (nonfluorescent) states, each on-off cycle corresponding to an enzymatic turnover. More than 500 on-off cycles are recorded in this trajectory. (**C**) Distribution of on-times (bars) derived from the trajectory in (B). The simulated curve (dashed line) is based on Eq. 4, assuming that $k_1 = 2.9 \pm 0.3\ s^{-1}$, $k_2 = 17 \pm 4\ s^{-1}$, and $k_{-1} = 0$. (**D**) Distribution of on-times (bars) derived from the emission trajectory of another single COx molecule recorded at 2 mM cholesterol. The simulated curve (dashed line) is based on Eq. 4, assuming $k_1 = 33 \pm 6\ s^{-1}$, $k_2 = 17 \pm 2\ s^{-1}$, and $k_{-1} = 0$. A factor of 10 increase in substrate concentration results in a factor of 11 ± 3 faster pseudo-first-order rate, k_1, which is consistent with the Michaelis-Menten mechanism in Eq. 2.

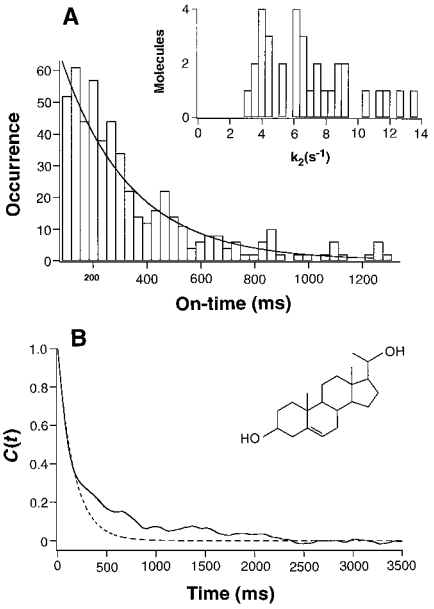

Fig. 2. (**A**) The on-time distribution derived from a single COx molecule with 2 mM 5-pregene-3β-20α-diol substrate (k_2 being the rate-limiting step). The solid line is an exponential fit with $k_2 = 3.9 \pm 0.5\ s^{-1}$. (**Inset**) The distribution of k_2 derived from on-time distributions of 33 COx molecules in the same sample. The static disorder of k_2 is evident. Note that k_2 are time averaged over the entire trajectories. (**B**) The normalized autocorrelation function of the fluorescence intensity from the COx molecule in (A), $\langle \Delta I(t) \Delta I(0) \rangle / \langle \Delta I(0)^2 \rangle$. The data (solid line) cannot be fitted well with a single exponential (dashed line). The structure of 5-pregene-3β-20α-diol substrate is shown in the inset.

straightforward analysis of the trajectories is the distribution of the on- and off-times. Similar trajectory analyses have been conducted in studies of single-ion channels with the patch-clamp technique (*28*). Figure 1C shows the on-time distribution, derived from a trajectory at a cholesterol concentration of 0.2 mM. A similar off-time distribution is also seen (*29*).

For a reversible chemical kinetic scheme

$$\underset{\text{on}}{\text{E-FAD}} \underset{k_b}{\overset{k_f}{\wedge}} \underset{\text{off}}{\text{E-FADH}_2} \quad (1)$$

the distribution of on-time (or off-time) should be an exponential function, with a time constant $1/k_f$ (or $1/k_b$) due to Poissonian statistics (*28*). In contrast, Fig. 1C shows a nonexponential distribution, which we attribute to a more complex kinetic scheme. In general, many two-substrate enzymes, such as COx, follow the "ping-pong" mechanism for the two-substrate binding processes, each obeying the Michaelis-Menten mechanism (*30*):

$$\underset{\text{on}}{\text{E-FAD}} + \text{S} \underset{k_{-1}}{\overset{k_1}{\wedge}} \underset{\text{on}}{\text{E-FAD}\bullet\text{S}} \overset{k_2}{\rightarrow} \underset{\text{off}}{\text{E-FADH}_2} + \text{P} \quad (2)$$

$$\underset{\text{off}}{\text{E-FADH}_2} + \text{O}_2 \underset{k'_{-1}}{\overset{k'_1}{\wedge}} \underset{\text{off}}{\text{E-FADH}_2\bullet\text{O}_2} \overset{k'_2}{\rightarrow} \underset{\text{on}}{\text{E-FAD}} + \text{H}_2\text{O}_2 \quad (3)$$

where S denotes the cholesterol substrate, and k_1 and k'_1 denote pseudo-first-order rates proportional to the concentrations of S and O_2, respectively. An assumption is made that other kinetic steps not shown in Eqs. 2 and 3, such as diffusion of product molecules out of the enzyme, are not rate limiting.

For COx, if we assume $k_{-1} = 0$, it follows from a kinetic analysis (*31*) that the probability distribution of on-times is the following:

$$p_{on}(t) = k_1 k_2/(k_2 - k_1)[\exp(-k_1 t) - \exp(-k_2 t)] \quad (4)$$

which is the convolution of two exponentials (k_1 and k_2). A similar expression of off-time distribution, $p_{off}(t)$, can be deduced for the $FADH_2$ oxidation reaction (Eq. 3).

Conventional enzymatic assays for two-substrate enzymes are often done by varying the concentration of one substrate while holding steady the concentrations of the others. The apparent Michaelis-Menten equations take a complex form (*30*). In order to study the half-reactions separately, the stop-flow technique is usually used. The in situ study of single-molecule turnover trajectories presented here allows the two half-reactions to be examined separately. We focused mostly on the FAD reduction half-reaction (Eq. 2).

A simulation of the $p_{on}(t)$ with Eq. 4 is plotted in Fig. 1C with $k_1 = 2.9 \pm 0.3\ s^{-1}$ and $k_2 = 17 \pm 4\ s^{-1}$. The nonexponential distribution arises because an intermediate (E-FAD•S) exists for the FAD reduction reaction (Eq. 2). When the concentration of the cholesterol substrate was increased from 0.2 mM to 2 mM, the on-time distribution (Fig. 1D) changed significantly whereas the off-time distribution remained unchanged. Simulation with Eq. 4 (Fig. 1D) yields $k_1 = 33 \pm 6\ s^{-1}$ and $k_2 = 17 \pm 2\ s^{-1}$. Note that the pseudo-first-order rate constant k_1 is increased by a factor of 11 ± 3. The analyses of on-time distribution confirm the existence of the intermediate for the FAD reduction reaction, which is consistent with the Michaelis-Menten mechanism (Eq. 2). Similarly, the off-time distribution (*29*) is also consistent with the Michaelis-Menten mechanism (Eq. 3).

We evaluated the static disorder, that is, the static heterogeneity of rates among individual molecules. To evaluate the static disorder of k_2, we made k_2 rate limiting. This condition is not quite achievable with a high concentration of cholesterol, but it is achievable with a high concentration of 5-pregene-3β-20α-diol substrate, a derivative of cholesterol (Fig. 2B, inset). The slower substrate results in a monotonic decay ($k_2 = 3.9 \pm 0.5\ s^{-1}$) in the on-time distribution for the COx molecule shown in Fig. 2A. A broad distribution of single exponential fits of k_2 for 33 COx molecules with the slow substrate (Fig. 2A, inset) is an apparently static disorder of k_2, with k_2 being the time averages along the entire trajectories (10 to 20 min) of the molecules. Static disorder has been observed for genetically identical and electrophoretically pure enzyme molecules (*5*, *6*) and has been postulated to arise from different conformers (*5*) or posttranslation modifications (*6*). Although the origin of the static disorder requires further investigation, we offer an alternative possibility for the COx system: proteolytic damages, such as oxidation, of the key residues of the enzyme (*32*).

Dynamic disorder (*33*), the fluctuation of reaction rate for a single molecule, is beyond the scope of conventional chemical kinetics. Chemical kinetics holds for Markovian processes (*34*), implying that an enzyme molecule undergoing a turnover exhibits no memory of its preceding turnovers. Dynamic disorder of proteins has been investigated in the context of single-molecule behavior with statistical theory (*35*) and molecular dynamics simulation (*36*). However, it is experimentally difficult, if not impossible, to distinguish static and dynamic disorder for chemical reactions in ensemble-averaged experiments. Statistical analyses of the turnover trajectories allow us to examine the validity of chemical kinetics at the single-molecule level and to distinguish static and dynamic disorders. To do so, we first chose the case of k_2 being the rate-limiting step (Fig. 2), so that the reaction scheme is reduced to Eq. 1, with forward and backward rates being $k_f = k_2$ and k_b, respectively.

Conventional kinetics experiments measure the relaxation of concentration of a large ensemble of molecules after a perturbation (such as fast mixing or a temperature jump). The fluctuation dissipation theorem applies to the reversible chemical reaction in Eq. 1 as follows (*37*):

$$\delta c(t)/\delta c(0) = \langle \Delta\zeta(0)\Delta\zeta(t)\rangle/\langle \Delta\zeta(0)^2\rangle \quad (5)$$

where $\delta c(t)$ is the concentration change of E-FAD measured in ensemble-averaged relaxation experiments, and $\zeta(t)$ is a dynamical variable for a single enzyme molecule in dynamic equilibrium; $\zeta = 1$ when the molecule is in the state of E-FAD, and $\zeta = 0$ when the molecule is in the state of $E\text{-}FADH_2$. The bracket denotes averaging along a stationary trajectory, and $\Delta\zeta(t) = \zeta(t) - \langle\zeta\rangle$. Thus, Eq. 5 relates the macroscopic experimental observable to the autocorrelation function of $\zeta(t)$, a microscopic property that has, to date, only been obtainable from molecular dynamics simulation. Our sin-

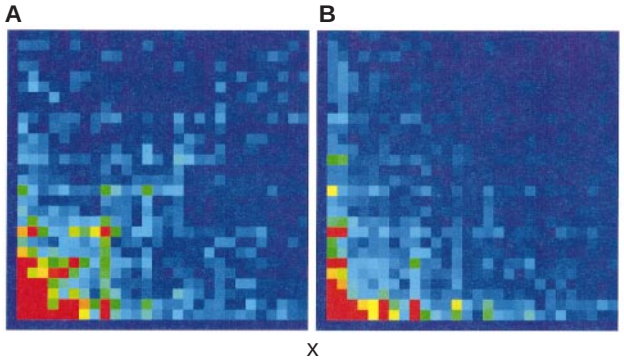

Fig. 3. The 2D conditional probability distribution for a pair of on-times (*x* and *y*) separated by a certain number of turnovers. The scale of *x* and *y* axes are from 0 to 1 s. (**A**) The 2D conditional histogram for on-times of two adjacent turnovers, which is derived from the trajectories of 33 COx molecules with 2 mM 5-pregene-3β-20α-diol substrate. A subtle diagonal feature is present. (**B**) The 2D conditional histogram for two on-times separated by 10 turnovers for the COx molecules in (A). The diagonal feature vanishes because the two on-times become independent of each other at the 10-turnover separation. The color code in (A) and (B) represents the occurrence (*z* axis) from 350 (red) to 0 (purple).

gle-molecule experiment allows the right side of Eq. 5 to be measured directly through the intensity autocorrelation function $\langle \Delta I(t)\Delta I(0)\rangle$. Figure 2B shows $\langle \Delta I(t)\Delta I(0)\rangle$ of the COx molecule in Fig. 2A.

According to chemical kinetics (*35*), $\delta c(t)/\delta c(0) = \exp[-(k_b + k_f)t]$, that is, a single exponential decay is expected for $\langle \Delta I(t)\Delta I(0)\rangle$, with a decay rate being the sum of the forward and backward rates. In fact, fluorescence intensity autocorrelation functions have been used to extract kinetics constants of chemical reactions with fluorescence correlation spectroscopy for a small number of molecules (*38*), and for one molecule at a time but averaging many molecules (*39*). The measured autocorrelation function (Fig. 2B, solid line) for a long trajectory of a single immobilized molecule was not a single exponential decay (Fig. 2B, dashed line). The multiexponential decay of the autocorrelation function can arise from the dynamic disorder of k_2 or k_f, or both, or from a more complex kinetic scheme (Eq. 3) than the backward reaction in Eq. 1.

The $p_{on}(t)$ in Fig. 2A has the advantage of only reflecting the forward reaction, but it does not have a good enough signal-to-noise ratio to reveal a multiexponential decay due to the dynamic disorder of k_2. Being a scrambled histogram, Fig. 2A is not sensitive to memory effects. We present a statistical analysis that provides definitive evidence for dynamic disorder in k_2. We evaluated the conditional probability distribution, $p(x,y)$, for pairs of on-times (x and y) separated by a certain number of turnovers. Two-dimensional (2D) histograms of a pair of on-times adjacent to each other (Fig. 3A) and separated by 10 turnovers (Fig. 3B) are shown for the sum of 33 COx molecules, thus reflecting the ensemble average of a single-molecule property. In the absence of dynamic disorder, the two on-times should be independent of each other, that is, $p(x,y) = p(x)p(y)$.

In contrast, Figs. 3A and 3B are clearly different, indicating a memory effect. For adjacent pairs of on-times (Fig. 3A), there is a diagonal feature, indicating that a short on-time tends to be followed by another short on-time, and a long on-time tends to be followed by another long on-time. For the separation of 10 turnovers (Fig. 3B), the distribution becomes independent. The memory effect arises from a slowly varying rate (k_2 being rate limiting). The rate equation for the forward reaction in Eq. 1 is written as

$$dP_{E\text{-}FAD}/dt = -k_2(t)P_{E\text{-}FAD} \qquad (6)$$

where $k_2(t)$ is a stochastic variable with a mean, $\langle k_2\rangle$. If the fluctuation of k_2 is very fast, $k_2(t)$ can be replaced by $\langle k_2\rangle$. Dynamic disorder arises when the time scale of the k_2 fluctuation is comparable to or slower than $1/k_2$. The fluctuation of $k_2(t)$ can be characterized by the k_2 variance and correlation time, that is, the memory time.

We quantitatively analyzed the visual difference between Figs. 3A and 3B by a covariance parameter (*40*, *41*) defined as

$$r(m) = \frac{n\sum_i^n t_i t_{i+m} - \left(\sum_i^n t_i\right)^2}{n\sum_i^n t_i^2 - \left(\sum_i^n t_i\right)^2} = \frac{\langle \Delta t(0)\Delta t(m)\rangle}{\langle \Delta t^2\rangle} \qquad (7)$$

where i is an index number for a total of $n + m$ turnovers in a trajectory; t_i is the experimentally determined on-time; and m is the separation between the pairs of on-times. Intuitively, $r = 1$ for a diagonal line, $r = -1$ for an off-diagonal line in the 2D distribution, and $r = 0$ for independent x and y. In fact,

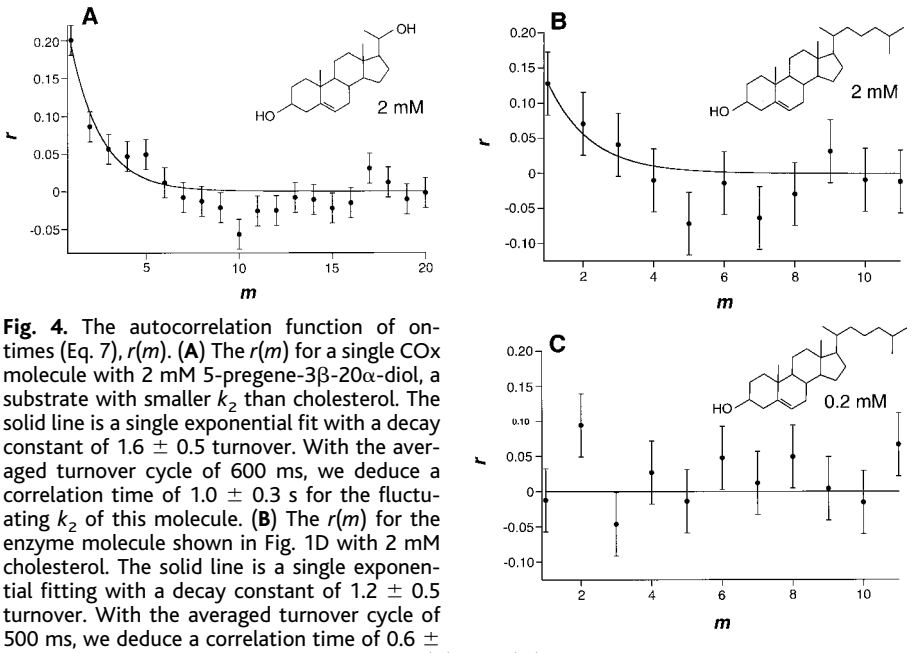

Fig. 4. The autocorrelation function of on-times (Eq. 7), $r(m)$. (**A**) The $r(m)$ for a single COx molecule with 2 mM 5-pregene-3β-20α-diol, a substrate with smaller k_2 than cholesterol. The solid line is a single exponential fit with a decay constant of 1.6 ± 0.5 turnover. With the averaged turnover cycle of 600 ms, we deduce a correlation time of 1.0 ± 0.3 s for the fluctuating k_2 of this molecule. (**B**) The $r(m)$ for the enzyme molecule shown in Fig. 1D with 2 mM cholesterol. The solid line is a single exponential fitting with a decay constant of 1.2 ± 0.5 turnover. With the averaged turnover cycle of 500 ms, we deduce a correlation time of 0.6 ± 0.3 s for the fluctuating k_2 of this molecule. (**C**) The $r(m)$ for the enzyme molecule shown in Fig. 1C with 0.2 mM cholesterol. The averaged turnover cycle of the trajectory is 900 ms. Under this condition k_1 is rate limiting. There is no dynamic disorder in k_1.

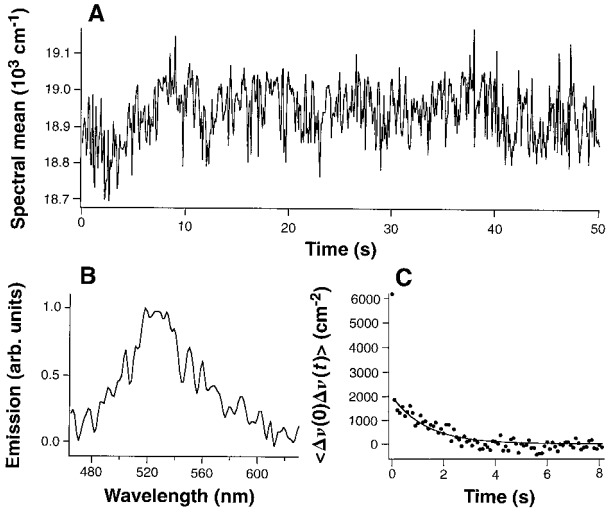

Fig. 5. (**A**) Trajectory of the spectral mean of a COx molecule in the absence of steroid substrate. Each data point is the first moment of the FAD emission spectrum sequentially recorded with a 100-ms data collection time. The spectral fluctuation is attributed to a spontaneous conformational fluctuation. (**B**) Emission spectrum of a COx molecule taken in 100 ms. The spectral mean of the spectrum is the first data point in (A). This and other spectra were taken by using a combination of a spectrograph (Acton Research, Acton, Massachusetts) and a cooled intensified charge-coupled device camera with Gen IV photocathode (Princeton Instruments, Trenton, New Jersey) and corrected for wavelength-dependent detection efficiency. (**C**) The correlation function (dots) of the spectral mean for the trajectory in (A). The first data point, a spike at zero time, is due to uncorrelated measurement noises and spectral fluctuations faster than the 100-ms time resolution. The solid line is a fit by a single exponential with a time constant of 1.3 ± 0.3 s, which coincides with the correlation time for k_2 fluctuation.

$r(m)$ is the autocorrelation function of the on-times (the last equality with the bracket denoting the trajectory average). In the absence of dynamic disorder, $r(0) = 1$ and $r(m) = 0$ ($m > 0$). In the presence of dynamic disorder, $r(m)$ is a decay with the initial ($m = 1$) amplitude reflecting the variance of k_2 and the decay time yielding the correlation time of k_2.

The $r(m)$ for a single enzyme molecule with 2 mM 5-pregene-3β-20α-diol (Fig. 4A) yields the correlation time of k_2, $\tau = 1.0 \pm 0.3$ s (1.6 turnovers in this trajectory). The fluctuation of k_2 was otherwise masked in the ensemble-averaged results, as well as in the scrambled 1D histogram [$p_{on}(t)$ in Fig. 2A]. We found every enzyme molecule in the system exhibited similar $r(m)$. The decay of $r(m)$ remained unchanged as the excitation intensity was doubled, so the phenomenon is not photoinduced. The high sensitivity of $r(m)$ to the memory effect allowed the observation of dynamic disorder even when cholesterol was the substrate (k_2 was not quite rate limiting). Figure 4B shows the decay of $r(m)$ for the molecule in Fig. 1D with 2 mM cholesterol. In contrast, the $r(m)$ for the molecule in Fig. 1C with 0.2 mM cholesterol remains zero (Fig. 4C) as k_1 becomes rate limiting. There is no dynamic disorder in k_1. For the $FADH_2$ oxidation half-reaction (Eq. 3), we found that the autocorrelation function for the off-times is zero for $m > 0$. In addition, there is no correlation between adjacent on- and off-times. Therefore, the $FADH_2$ oxidation reaction (k'_1 and k'_2) involving oxygen does not exhibit dynamic disorder.

We attribute the fluctuation of k_2 to conformational fluctuation of the protein, which can be probed by the emission spectra of the FAD active site. Figure 5A shows a trajectory of the spectral mean of the emission spectra of a single enzyme molecule in the absence of cholesterol substrate molecules. The slow fluctuation of the emission spectrum (Fig. 5B) reflects conformational changes around the FAD, a phenomenon that is otherwise hidden in ensemble-averaged measurements. Similar room-temperature spectral fluctuation of single dye molecules in polymer has been studied in detail, providing information regarding the energy landscape (*15*). The autocorrelation function of the spectral mean trajectory is shown in Fig. 5C. The decay curve was independent of excitation rate, indicating a spontaneous (rather than photoinduced) conformational fluctuation. Interestingly, the decay constant is 1.3 ± 0.3 s, which is on the same time scale as the correlation time of k_2, τ. This provides strong evidence that conformational fluctuation results in variation of the enzymatic rate k_2.

The simplest model that can account for the fluctuation of k_2 involves two conformational states of the enzyme, E and E′, which have different rates (k_{21} and k_{22}) for the activation step and interchange with a rate $1/\tau = k_E + k_{E'}$ slower than $\langle k_2 \rangle$:

$$\begin{array}{ccc} & k_E & \\ E & \wedge & E' \\ & k_{E'} & \end{array}$$

$$\begin{array}{ccccc} & & k_1 & & k_{21} \\ E\text{-}FAD + S & \wedge & E\text{-}FAD{\bullet}S & \rightleftarrows & E\text{-}FADH_2 + P \\ & & k_{-1} & & \\ \Updownarrow & & \Updownarrow & & \Updownarrow \end{array}$$

$$E'\text{-}FAD + S \underset{k_{-1}}{\overset{k_1}{\wedge}} E'\text{-}FAD{\bullet}S \rightleftarrows E'\text{-}FADH_2 + P \quad (8)$$

A simulation of $r(m)$ based on this kinetic scheme assuming $k_E/k_{E'} = 1$ and $k_{21}/k_{22} = 5$ matches the experimental curve (Fig. 4A), indicating a substantial difference in k_{21} and k_{22} (*42*). We note that the dynamic disorder of k_2 for the Michaelis-Menten mechanism (Eq. 2), a non-Markovian behavior, can be accounted for by the more complicated kinetics scheme (Eq. 8) with the constant rates k_{21} and k_{22}.

Similar molecular memory phenomena deviating from the Michaelis-Menten mechanism have been inferred previously by ensemble-averaged experiments for other monomeric enzyme systems (*43*). A consequence of the memory effect is a sigmoidal dependence of the enzymatic reaction velocity on the substrate concentration. It was postulated that such "kinetic cooperativity" of the monomeric enzymes facilitates physiological regulation. Interestingly, a sigmoidal dependence on cholesterol concentration was reported for COx (*27*), which could be related to our finding of the memory effect.

Although the two-state model suffices to account for the fluctuation of k_2 and the spectral mean, there can be more than two conformational states, or even a broad distribution of conformational states (*44*) with distinctly different k_2. For the two-state model, a simple kinetic scheme for the interconverting conformers can account for the dynamics (*45*). For the continuous model, a diffusive motion along a conformational coordinate perpendicular to the reaction coordinate induces a fluctuating barrier height (*46*). On the basis of this model, a simulation of the stochastic trajectory and its $r(m)$ yields the k_2 variance, $\langle k_2^2 \rangle = 12.5$ s^{-2} (*42*), corresponding to a significant amplitude of fluctuation (standard deviation being 70% of $\langle k_2 \rangle$) (*47*). Detailed microscopic pictures of conformational dynamics and its influence on enzymatic reactions are expected to emerge from single molecule studies.

References and Notes

1. For a recent review, see X. S. Xie and J. K. Trautman, *Annu. Rev. Phys. Chem.* **59**, 441 (1998).
2. For a review, see S. Nie and R. N. Zare, *Annu. Rev. Biophys. Biomol. Struct.* **26**, 567 (1997).
3. J. J. Macklin, J. K. Trautman, T. D. Harris, L. E. Brus, *Science* **272**, 255 (1996).
4. T. Ha, T. Enderle, D. S. Chemla, P. R. Selvin, S. Weiss, *Phys. Rev. Lett.* **77**, 3979 (1996).
5. Q. F. Xue and E. S. Yeung, *Nature* **373**, 681 (1995).
6. D. B. Craig, E. A. Arriaga, J. C. Y. Wong, H. Lu, N. J. Dovichi, *J. Am. Chem. Soc.* **118**, 5245 (1996).
7. H. P. Lu and X. S. Xie, *J. Phys. Chem. B* **101**, 2753 (1997).
8. L. Edman, U. Mets, R. Rigler, *Proc. Natl. Acad. Sci. U.S.A.* **93**, 6710 (1996).
9. Y. Jia *et al.*, *ibid.* **94**, 7932 (1997).
10. E. Geva and J. L. Skinner, *Chem. Phys. Lett.* **288**, 255 (1998).
11. T. Schmidt, G. J. Schutz, W. Baumgartner, H. J. Gruber, H. Schindler, *J. Phys. Chem.* **99**, 17662 (1995).
12. R. M. Dickson, D. J. Norris, Y.-L. Tzeng, W. E. Moerner, *Science* **274**, 966 (1996).
13. X.-H. Xu and E. S. Yeung, *ibid.* **275**, 1106 (1997).
14. T. Ha, J. Glass, T. Enderle, D. S. Chemla, S. Weiss, *Phys. Rev. Lett.* **80**, 2093 (1998).
15. H. P. Lu and X. S. Xie, *Nature* **385**, 143 (1997).
16. S. Wennmalm, L. Edman, R. Rigler, *Proc. Natl. Acad. Sci. U.S.A.* **94**, 10641 (1997).
17. R. M. Dickson, A. B. Cubitt, R. Y. Tsien, W. E. Moerner, *Nature* **388**, 355 (1997).
18. D. A. Vanden Bout *et al.*, *Science* **277**, 1074 (1997).
19. T. Funatsu, Y. Harada, M. Tokunaga, K. Saito, T. Yanagida, *Nature* **374**, 555 (1995); A. Ishijima *et al.*, *Cell* **92**, 161 (1998).
20. R. D. Vale *et al.*, *Nature* **380**, 451 (1996).
21. H. Noji, R. Yasuda, M. Yoshida, K. Kinosita, *ibid.* **386**, 299 (1997).
22. For reviews, see S. Ghisla and V. Massey, *Eur. J. Biochem.* **181**, 1 (1989); F. Muller, *Chemistry and Biochemistry of Flavoenzymes* (CRC Press, Boca Raton, FL, 1992), vol. I.
23. A. Vrielink, L. F. Lloyd, D. M. Blow, *J. Mol. Biol.* **219**, 533 (1991).
24. COx of *Brevibacterium* sp. was purchased from Sigma (St. Louis, MO). The enzyme was suspended in 0.5 ml of 20 mM potassium phosphate (KPi) buffer, pH 7.0, and injected onto Superdex 200 HR 10/30 gel filtration column (Pharmacia, Piscataway, NJ) equilibrated at 20 mM KPi buffer (pH 7.0) with 100 mM NaCl. Proteins were eluted with the same buffer by a fast protein liquid chromatography system (Pharmacia). COx activity was eluted with a major peak. SDS–polyacrylamide gel electrophoresis analysis of the fractions containing the peak showed a single protein band with a molecular size of about 53 kD. The sample was prepared by first spin-coating a buffered solution (pH 7.4) of agarose (1% by weight, Type VII, Sigma) above the gelling temperature (30°C) on two glass cover slips (Clay Adams and Fisher Scientific) to form thin layers (<1 μm). The two coated glass cover slips were then used to sandwich a thin layer (5 to ~20 μm) of the same gel containing diluted enzyme molecules (10^{-10} M). The gel formed in a few minutes after cooling from the gel temperature.
25. X. S. Xie and R. C. Dunn, *Science* **265**, 361 (1994).
26. T. Uwajima, H. Yagi, O. Terada, *Agric. Biol. Chem.* **38**, 1149 (1974); A. G. Smith and C. J. W. Brooks, *J. Steroid Biochem.* **7**, 705 (1976).
27. T. Vasudevan and T. Zhou, *Appl. Biochem. Biotechnol.* **60**, 63 (1996).
28. For a review, see D. Colquhoun and A. G. Hawkes, in *Single-Channel Recording*, B. Sakamann and E. Neher, Eds. (Plenum, New York, ed. 2, 1995), pp. 397–482.
29. H. P. Lu and X. S. Xie, data not shown.
30. See, for example, T. Palmer, *Understanding Enzymes* (Prentice-Hall, New York, ed. 4, 1991), chap. 9.
31. For single molecules, the kinetic equations for Eq. 2 are written in terms of probabilities for finding (instead of concentrations of) the species at time t (with $t = 0$ being the onset of the on-time):

$$dP_{E\text{-}FAD}(t)/dt = -k_1 P_{E\text{-}FAD}(t) + k_{-1} P_{E\text{-}FAD\bullet S}(t) \quad (9)$$

$$dP_{E\text{-}FAD\bullet S}(t)/dt = k_1 P_{E\text{-}FAD}(t) - (k_{-1} + k_2) P_{E\text{-}FAD\bullet S}(t) \quad (10)$$

$$dP_{E\text{-}FADH_2}(t)/dt = k_2 P_{E\text{-}FAD\bullet S}(t) \quad (11)$$

The initial conditions for solving the coupled differential equations are $P_{E\text{-}FAD}(0) = 1$, $P_{E\text{-}FAD\bullet S}(0) = 0$, $P_{E\text{-}FADH_2}(0) = 0$ at $t = 0$. We evaluate the probability distribution of on-times, $p_{on}(t)$. The probability for an on-time between t and $t + \Delta t$ is $p_{on}(t)\Delta t$, which is the same as the probability of having the emission switched off between t and $t + \Delta t$, $\Delta P_{E\text{-}FADH_2}(t) = k_2 P_{E\text{-}FAD\bullet S}(t)\Delta t$. Explicitly, $p_{on}(t) = dP_{E\text{-}FADH_2}(t)/dt = k_2 P_{E\text{-}FAD\bullet S}(t)$. Solving Eqs. (9) and (10) for $P_{E\text{-}FAD\bullet S}(t)$ by Laplace transform yields

$$p_{on}(t) = k_1 k_2 / 2a\{\exp[(a + b)t] - \exp[(b - a)t]\} \quad (12)$$

where $a = \sqrt{[¼(k_1 + k_{-1} + k_2)^2 - k_1 k_2]}$ and $b = -½(k_1 + k_{-1} + k_2)$.

32. In contrast, we found there is no static disorder in k_1, because k_1 are the same among individual molecules measured at low concentration of the cholesterol substrate (k_1 being rate limiting). Similarly, the off-time distributions for individual molecules are found to be identical to each other. Therefore, there is no static disorder for the $FADH_2$ oxidation half-reaction (Eq. 3).
33. For a review, see R. Zwanzig, *Acc. Chem. Res.* **23**, 148 (1990).
34. N. G. van Kampen, *Stochastic Processes in Physics and Chemistry* (Elsevier, Amsterdam, Netherlands, 1992).
35. J. Wang and P. Wolynes, *Phys. Rev. Lett.* **74**, 4317 (1995); *J. Chem. Phys.*, in press.
36. J. N. Gehlen, M. Marchi, D. Chandler, *Science* **263**, 499 (1994).
37. D. Chandler, *Introduction to Modern Statistical Mechanics* (Oxford Univ. Press, Oxford, 1987), chap. 8.
38. D. Magde, E. Elson, W. W. Webb, *Phys. Rev. Lett.* **29**, 705 (1972).
39. M. Eigen and R. Rigler, *Proc. Natl. Acad. Sci. U.S.A.* **91**, 5740 (1994).
40. See, for example, E. Mansfield, *Basic Statistics with Applications* (Norton, New York, 1986), chap. 11.
41. The covariance parameter for x and y is

$$\frac{n\sum_i^n x_i y_i - \left(\sum_i^n x_i\right)\left(\sum_i^n y_i\right)}{\sqrt{\left[n\sum_i^n x_i^2 - \left(\sum_i^n x_i\right)^2\right]\left[n\sum_i^n y_i^2 - \left(\sum_i^n y_i\right)^2\right]}} \quad (13)$$

42. G. Schenter, H. P. Lu, X. S. Xie, in preparation.
43. For reviews, see K. E. Neet and G. R. Anislie, *Methods Enzymol.* **64**, 192 (1980); C. Frieden, *Annu. Rev. Biochem.* **48**, 471 (1979); J. Ricard, J. Meunier, J. Buc, *Eur. J. Biochem.* **49**, 195 (1974).
44. H. Frauenfelder, S. G. Sligar, P. G. Wolynes, *Science* **254**, 1598 (1991).
45. B. M. Hoffman and M. A. Ratner, *J. Am. Chem. Soc.* **109**, 6237 (1987).
46. N. Agmon and J. J. Hopfield, *J. Chem. Phys.* **78**, 6947 (1983).
47. It is also possible that the conformational changes are induced by substrate binding, the redox reactions, or both, which can either lead to new conformational states or shift the equilibrium between the existing conformation states (*43*). Our single-molecule data can neither prove nor disprove this possibility at this point.
48. We thank G. Schenter, L. Mets, P. Barbara, and P. Mendes for helpful discussions. Supported by Chemical Sciences Division of the Office of Basic Energy Sciences and the Office of Biological and Environmental Research within the Office of Energy Research of U.S. Department of Energy (DOE), and in part by a Laboratory Directed Research and Development fund at Pacific Northwest National Laboratory, which is operated for DOE by Battelle Memorial Institute.

15 July 1998; accepted 30 October 1998

Frequency Tuning of Basilar Membrane and Auditory Nerve Fibers in the Same Cochleae

S. Shyamla Narayan, Andrei N. Temchin, Alberto Recio, Mario A. Ruggero*

Responses to tones of a basilar membrane site and of auditory nerve fibers innervating neighboring inner hair cells were recorded in the same cochleae in chinchillas. At near-threshold stimulus levels, the frequency tuning of auditory nerve fibers closely paralleled that of basilar membrane displacement modified by high-pass filtering, indicating that only relatively minor signal transformations intervene between mechanical vibration and auditory nerve excitation. This finding establishes that cochlear frequency selectivity in chinchillas (and probably in mammals in general) is fully expressed in the vibrations of the basilar membrane and renders unnecessary additional ("second") filters, such as those present in the hair cells of the cochleae of reptiles.

In mammalian cochleae, the bulk of auditory information is transmitted to the brain via the inner hair cells, which provide the sole synaptic inputs to 90% to 95% of the afferent fibers of the auditory nerve (*1*). Auditory nerve excitation is triggered by depolarization of inner hair cells upon deflection of their "hair" bundles toward the taller stereocilia (*2*, *3*). Presumably, the forces that deflect the stereocilia bundles are derived from the vibrations of the basilar membrane (BM), but it is not known how these vibrations are transmitted to the inner hair cells (*4*). Although the BM and auditory nerve fibers are similarly tuned at frequencies close to the characteristic frequency (CF) (*5*–*9*), there is no consensus about whether neural threshold corresponds to a constant magnitude of BM displacement, velocity, or some function of these variables.

Until now, comparisons of the response properties of auditory nerve fibers or inner hair cells and the BM have been indirect, involving data from different subjects [with one exception (*10*)]. For example, a frequency-threshold tuning curve recorded from a single auditory nerve fiber in one subject was compared with BM data from another individual of the same species (*5*–*7*). Alternatively, comparisons have been based on averaged data obtained from two different groups of subjects (*8*). Considering the variability of both neural [for example, see (*11*)] and mechanical responses [for example, see (*5*, *9*)], and also the different measurement conditions, such comparisons are bound to lead to imprecise conclusions. To clarify how mechanical vibrations are translated into neural spike trains, we conducted experiments that previously were not successful. We recorded sequentially, under identical conditions, the responses to tones of a BM site and of auditory nerve fibers innervating neighboring inner hair cells in the nearly normal ears of two anesthetized chinchillas (*12*).

The magnitudes of mechanical and neural responses as a function of stimulus frequency were compared by using tuning curves, which plot the stimulus levels at which a fixed response criterion is reached. In one cochlea, four fibers were encountered with CFs (9.5, 9.3, 8.0, and 7.8 kHz) comparable to the CF of the BM recording site (9.5 kHz). The fiber CFs indicate that they terminated very near the BM recording site or about 0.08, 0.64, and 0.72 mm away, respectively (*13*). Figure 1A shows tuning curves for the BM and one fiber, selected because its CF coincided with that of the BM site and could be compared with the BM tuning curve directly. At the fiber's CF threshold [13-dB sound pressure level (SPL)], BM vibrations had a peak displacement of 2.7 nm or, equivalently, a peak velocity of 164 μm/s. These values were used to plot isodisplacement and isovelocity tuning curves. At frequencies between CF and 1 kHz, there was a good match between neural thresholds and a constant BM velocity. When the entire frequency range of measurements was considered, however, neural thresholds were better fit by mechanical displacements subjected to high-pass filtering at a rate of 3.8 dB per octave. The other three fibers had similar tuning curves, which were well fit (after normalization to the BM CF) by BM displacement high-pass filtered at rates of 4.0, 3.9, and 4.1 dB per octave (*14*).

In another cochlea, the BM recording site had a CF of 9 kHz and four fibers were found with comparable CFs (9.25, 8.7, 8.1, and 8.0 kHz) and probable terminations 0.10, 0.14,

S. S. Narayan, A. N. Temchin, M. A. Ruggero, The Hugh Knowles Center, Audiology and Hearing Sciences Program, Department of Communication Sciences and Disorders, and Institute for Neuroscience, Northwestern University, Evanston, IL 60208–3550, USA. A. Recio, Department of Physiology, University of Wisconsin, Madison, WI 53706, USA.

*To whom correspondence should be addressed. E-mail: mruggero@nwu.edu